

Supporting Information

**Theoretical Study on Conformation Dynamics of Three-Station
Molecular Shuttle in Different Environments and its Influence on
NMR Chemical Shifts and Binding Interactions**

Pingying Liu^{a,b}, Wei Li^a, Li Liu^a, Leyong Wang^a and Jing Ma^{a,*}

^aSchool of Chemistry and Chemical Engineering, Key Laboratory of Mesoscopic Chemistry of MOE, Nanjing University, Nanjing 210093, People's Republic of China

^bSchool of Materials Science and Engineering, Jingdezhen Ceramic Institute, Jingdezhen 333403, China

*Corresponding author: majing@nju.edu.cn, Fax: 86-25-83596131, Tel: 86-25-83597408

Contents

1. DFT computational details.	S3
2. Table S1 for the MD simulation details.	S4
3. Figure S1 for the calculated BSSE-binding energies and electrostatic potential maps of macrocycles and threads at M06-2X/6-31G(d, p) level based on the ten energetically low-lying conformations extracted for MD simulation of interlocked [2]rotaxane at Station I.	S5
4. Figure S2. The optimized geometries for three stations with six different functionals.	S6
5. Figure S3. The optimized geometries for pseudorotaxanes at B3LYP/6-31G (d, p) level.	S7
6. Table S2 for hydrogen bond lengths, $d_{O...H}$, and stabilization energies obtained from second order perturbation, $E^{(2)}$, for H-bonding interactions of [2]rotaxane interlocking at different stations based on the NBO analysis.	S8
7. Figure S4. The calculated 1H NMR chemical shifts for two degenerate	

- molecular shuttle conformations (binding at Station I). S9
8. Figure S5 for MD trajectories of molecular shuttle binding at Station I in different solvents. S10
9. Figure S6 for the molecular shuttle binding at Station I: (a) comparison of the differences of computed ^1H NMR chemical shifts using different DFT functionals with 6-31G (d, p) basis set with respect to the M06-2X functional results.(b)convergence test (along MD trajectory) of the calculated NMR chemical shifts of the protons attaching at Station I. S11
10. Table S3 for the calculated ^1H NMR chemical shifts with PCM model and explicit solvent model (MD ensemble-average) for molecular shuttle binding at station I at M06-2X/6-31G(d, p) level. S12
11. Figure S7 for the radial distribution function of 1ns snapshot of MD simulation of Station I. S13

1. DFT functionals

All the structures were optimized using the density functional theory (DFT)¹ method with 6-31G(d,p)² basis sets. The B3LYP functional includes Becke's three-parameter-exchange functional and Lee-Young-Parr correlation functional³, CAM-B3LYP⁴ is the long range corrected version of B3LYP using the Coulomb-attenuating method, PBEPBE⁵, uses 25% exchange and 75% correlation weighting. mPW1PW91⁶ uses Perdew-Wang exchange as modified by Adamo and Barone combined with PW91 correlation. M06-2X⁷ is a hybrid meta-functional that contains 27% HF exchange, parameterized using delocalized system, and WB97X-D⁸ includes empirical dispersion and long range corrections.

reference:

1. P. Hohenberg, W. Kohn, Phys. Rev. **1964**, 136B, 864-871.
2. M.M. Franchl, W.J. Pietro, W.J. Hehre, J.S. Binkley, M.S. Gordon, D.J. DeFrees, J.A. Pople J. Chem. Phys. **77**, 3654-3665 (1982).
3. a) A. D. Becke, J. Chem. Phys. **1993**, **98**, 5648-5652. b) C. Lee, W. Yang, R. G. Parr, Phys. Rev. B **1988**, **37**, 785-789. c) R.G., Parr, W. Yang, Density Functional Theory of Atoms and Molecules, Oxford, New York, **1989**.
4. T. Yanai, D. Tew, and N. Handy, "A new hybrid exchange-correlation functional using the Coulomb-attenuating method (CAM-B3LYP)," *Chem. Phys. Lett.*, **393** (2004) 51-57.
5. (a) C. Adamo and V. Barone, "Toward reliable density functional methods without adjustable parameters: The PBE0 model," *J. Chem. Phys.*, **110** (1999) 6158-69 (b) J. P. Perdew, K. Burke, and M. Ernzerhof, "Generalized gradient approximation made simple," *Phys. Rev. Lett.*, **77** (1996) 3865-68. (c) J. P. Perdew, K. Burke, and M. Ernzerhof, "Errata: Generalized gradient approximation made simple," *Phys. Rev. Lett.*, **78** (1997) 1396.
6. C. Adamo and V. Barone, "Exchange functionals with improved long-range behavior and adiabatic connection methods without adjustable parameters: The mPW and mPW1PW models," *J. Chem. Phys.*, **108** (1998) 664-75.
7. Y. Zhao and D. G. Truhlar, "The M06 suite of density functionals for main group thermochemistry, thermochemical kinetics, noncovalent interactions, excited states, and transition elements: two new functionals and systematic testing of four M06-class functionals and 12 other functionals," *Theor. Chem. Acc.*, **120** (2008) 215-41.
8. J.-D. Chai and M. Head-Gordon, "Long-range corrected hybrid density functionals with damped atom-atom dispersion corrections," *Phys. Chem. Chem. Phys.*, **10** (2008) 6615-20.

Table S1. The details for the solvent models used in molecular dynamics simulations.

	MD averaged	MD@CD ₃ CN-CDCl ₃	MD@CDCl ₃	MD@	MD@mix
	@solution	solvents	solvents	vacuum	solvents
Solute	1	1	1	1	1
Solvents					
CD ₃ CN	1777	1777	0	0	1777
CDCl ₃	1223	1223	3000	0	1223

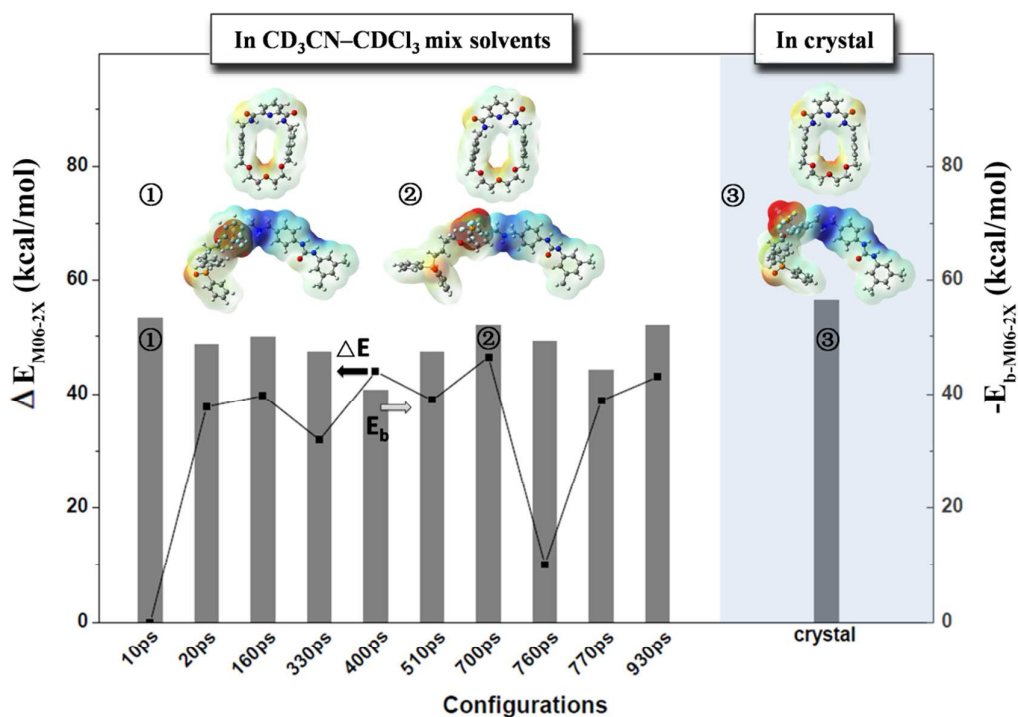


Figure S1. The relative energy, ΔE_{M06-2X} , and BSSE-binding energies, $-E_{b-M06-2X}$, and electrostatic potential maps of macrocycles and threads at M06-2X/6-31G(d, p) level based on the ten energetically low-lying conformations extracted from MD simulation of interlocked [2]rotaxane at Station I. The 10ps structure has the lowest energy with $\Delta E_{M06-2X}=0$. Computational results using the crystal structure were also given for comparison.

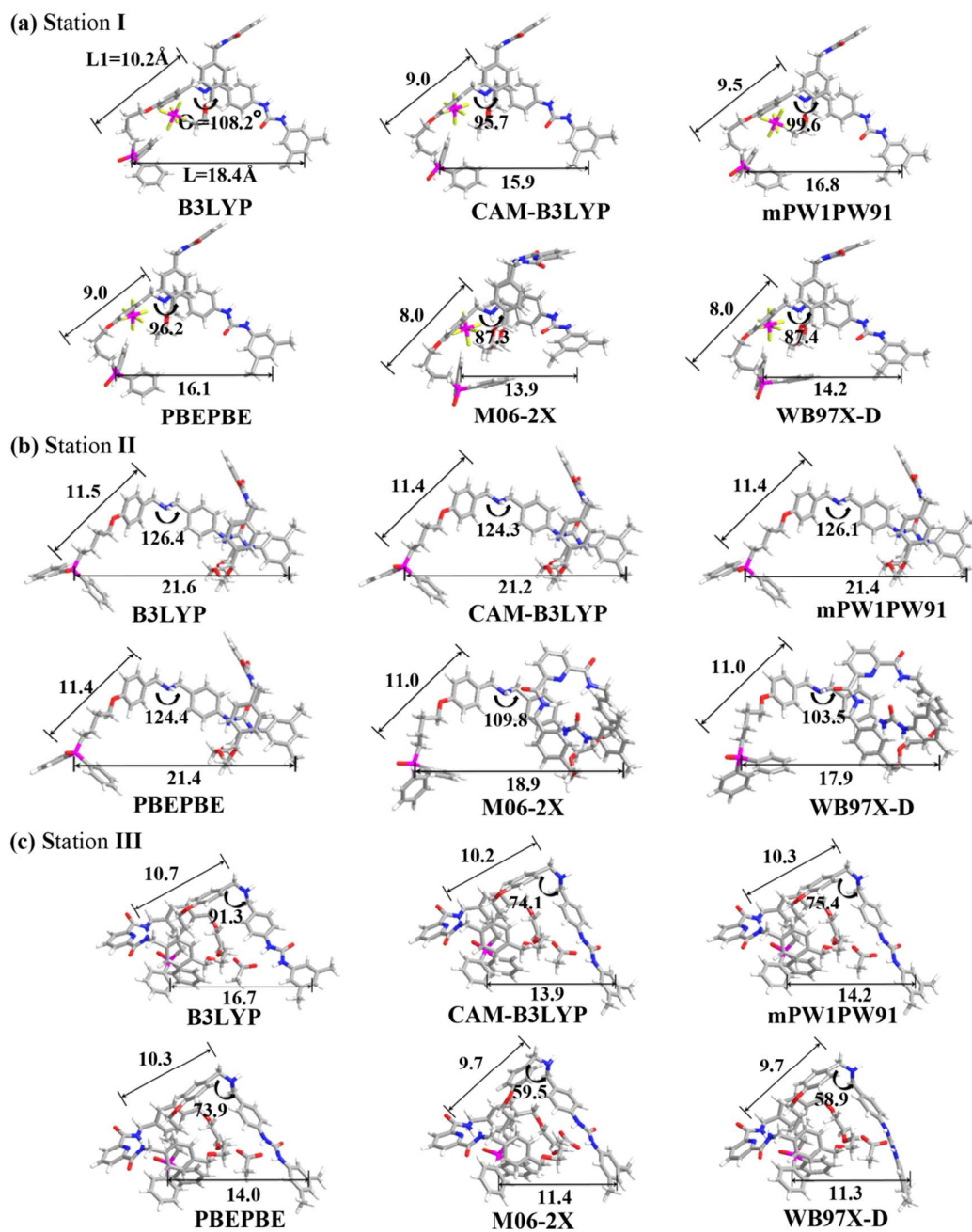
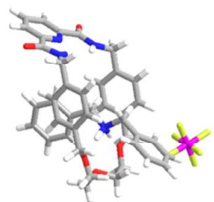


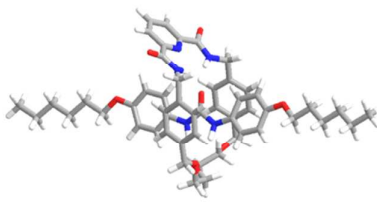
Figure S2. The optimized geometries and geometrical parameters of thread for three stations with six different functionals.

Pseudorotaxane

(a) DBA⁺- based(Station I)



(b) Urea-based(Station II)



(c) Phosphine oxide-based(Station III)

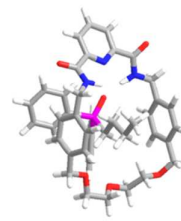
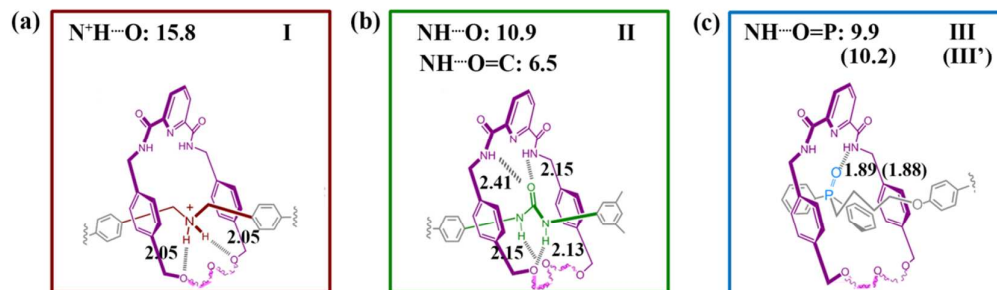


Figure S3. The optimized geometries for pseudorotaxanes at M062X/6-31G (d, p) level.

Table S2. Hydrogen bond lengths, $d_{O...H}$, and stabilization energies obtained from second order perturbation, $E^{(2)}$, for H-bonding interactions of [2]rotaxane interlocking at different stations based on the NBO analysis.



	Donor	Type	Acceptor	Type	$d_{O...H}$ (Å)	Interaction	$E^{(2)}$ (kcal/mol)
I-HB1	O 151	LP (2)	N83 – H85	BD*(1)	2.05	$n_O \rightarrow \sigma_{N-H}^*$	7.58
I-HB2	O 153	LP (2)	N83 – H84	BD*(1)	2.05	$n_O \rightarrow \sigma_{N-H}^*$	7.80
I-HB3	O 152	LP (2)	C22 – H23	BD*(1)	2.32	$n_O \rightarrow \sigma_{CH}^*$	1.08
II-HB1	O50	LP (1)	N130-H131	BD*(1)	2.13	$n_O \rightarrow \sigma_{N-H}^*$	7.19
II-HB2	O57	LP (2)	N126-H127	BD*(1)	2.15	$n_O \rightarrow \sigma_{N-H}^*$	3.73
II-HB3	O129	LP (2)	N14-H150	BD*(1)	2.15	$n_O \rightarrow \sigma_{N-H}^*$	5.08
II-HB4	O129	LP (2)	N15-H16	BD*(1)	2.41	$n_O \rightarrow \sigma_{N-H}^*$	1.43
III-HB1	O90	LP (1)	N14-H150	BD*(1)	1.89	$n_O \rightarrow \sigma_{N-H}^*$	9.88

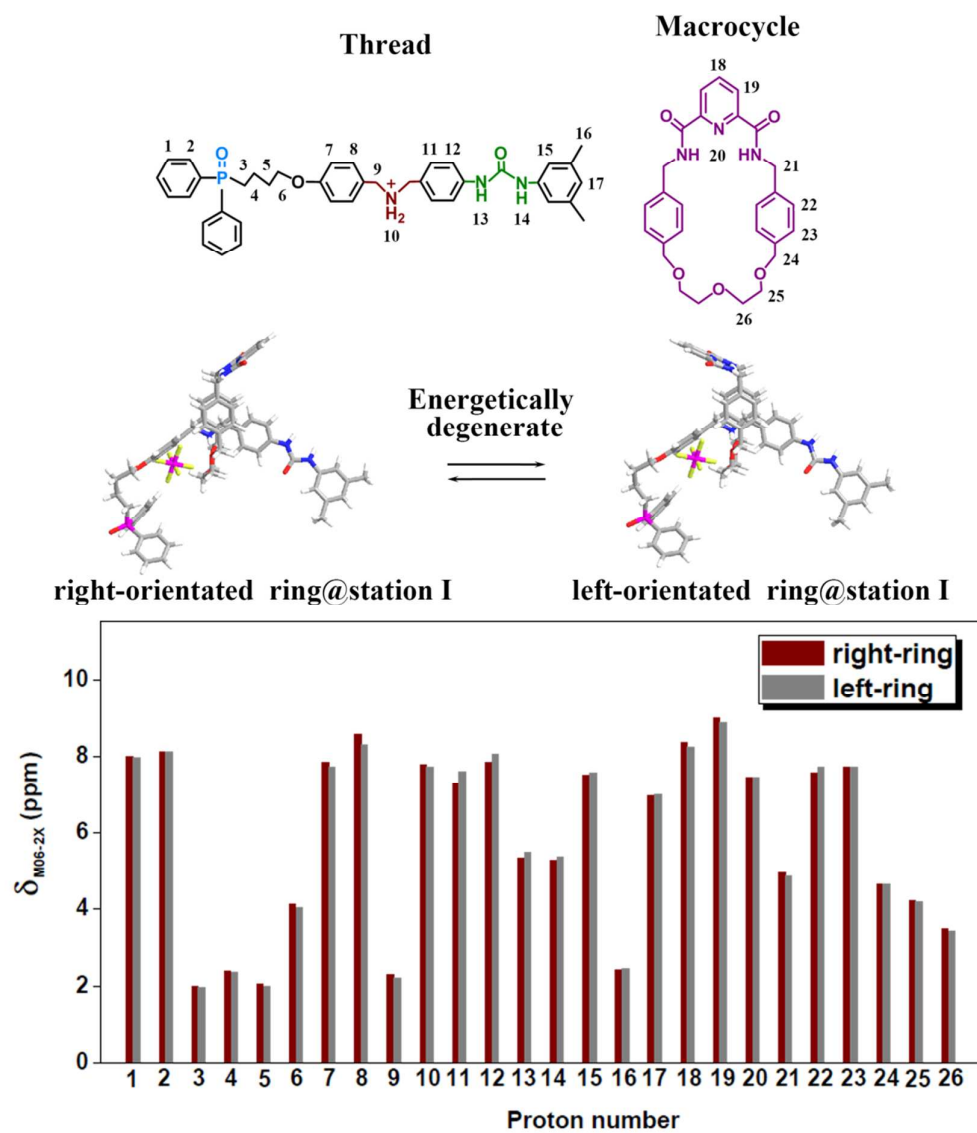


Figure S4. The calculated ^1H NMR chemical shifts for two degenerate molecular shuttle conformations (binding at Station I).

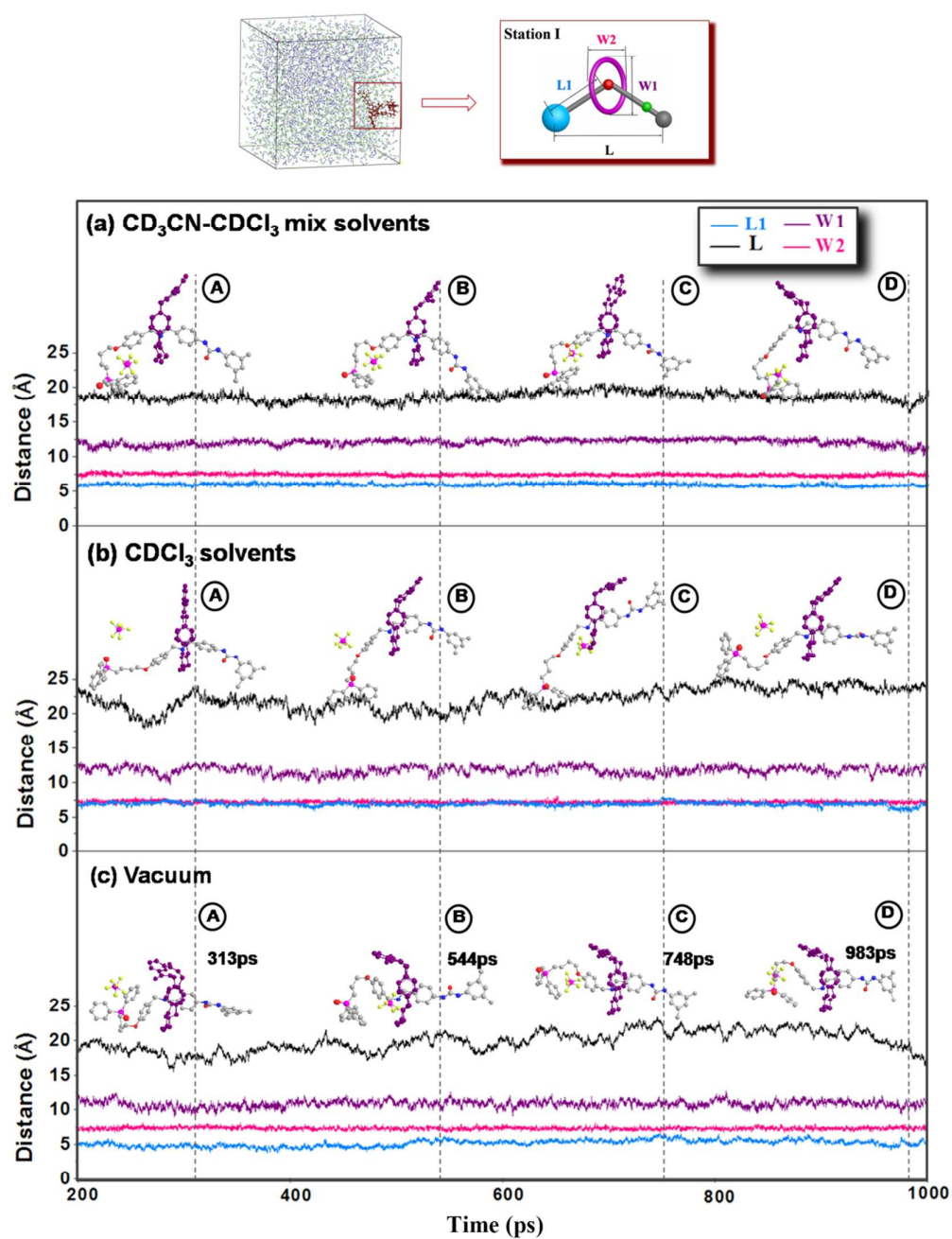


Figure S5. MD trajectories of molecular shuttle binding at Station I in (a) $\text{CD}_3\text{CN}-\text{CDCl}_3$ mix solvents (b) nonpolar CDCl_3 solvents (c) vacuum without any solvents.

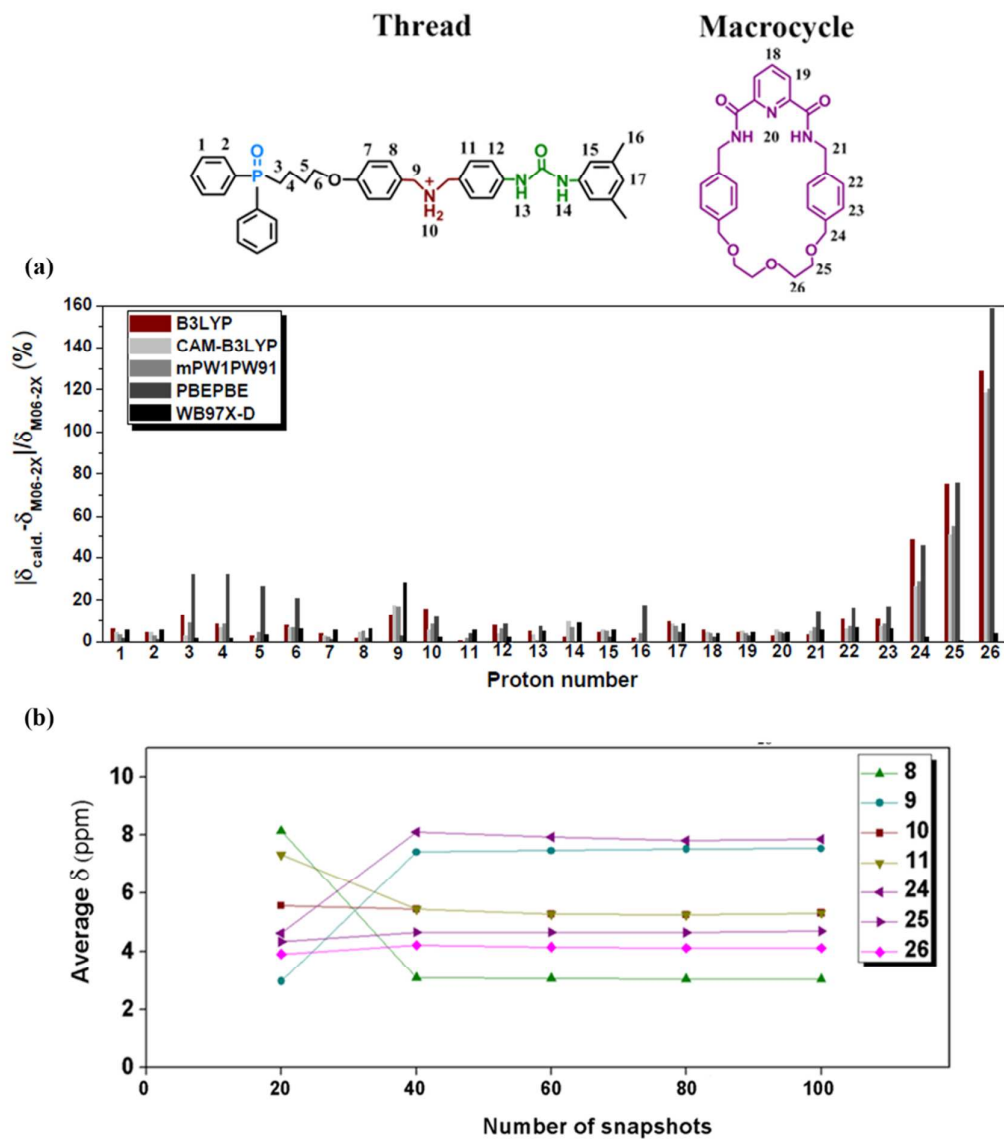


Figure S6. For the molecular shuttle binding at Station **I**: (a) comparison of the differences of computed ^1H NMR chemical shifts using different DFT functionals with 6-31G (d, p) basis set with respect to the M06-2X functional results; (b) convergence test (along MD trajectory) of the calculated NMR chemical shifts of the protons attaching at Station **I**.

Table S3. The calculated ^1H NMR chemical shifts with PCM model and explicit solvent model (MD ensemble-average) for molecular shuttle binding at Station **I** at M06-2X/6-31G(d, p) level.

NO.H	PCM solvent=CH ₃ CN	PCM solvent=CHCl ₃	Solu. ^{MD}	Exp.
1	8.82	8.70	8.70	7.54
2	8.90	8.86	9.07	7.76
3	3.97	3.85	2.47	2.37
4	3.03	3.20	2.47	1.78
5	2.78	2.71	2.49	1.85
6	5.14	5.19	4.54	3.91
7	8.52	8.50	8.53	6.65
8	9.28	9.16	8.44	6.95
9	3.98	3.87	2.95	2.50
10	6.46	6.50	5.24	7.20
11	8.50	8.42	8.10	6.96
12	8.54	8.52	8.46	7.36
13	4.91	4.69	5.20	7.51
14	6.03	5.76	5.03	7.27
15	8.16	8.12	7.87	7.03
16	2.5	2.49	2.72	2.25
17	8.37	8.34	7.75	6.66
18	9.44	9.42	9.30	8.17
19	9.34	9.38	9.43	8.43
20	9.29	9.04	7.73	9.01
21	4.95	4.93	5.16	4.65
22	8.57	8.52	8.51	7.08
23	8.26	8.26	8.56	6.83
24	4.99	4.96	4.62	4.21
25	3.92	3.89	4.04	3.59
26	4.65	4.71	4.02	3.25

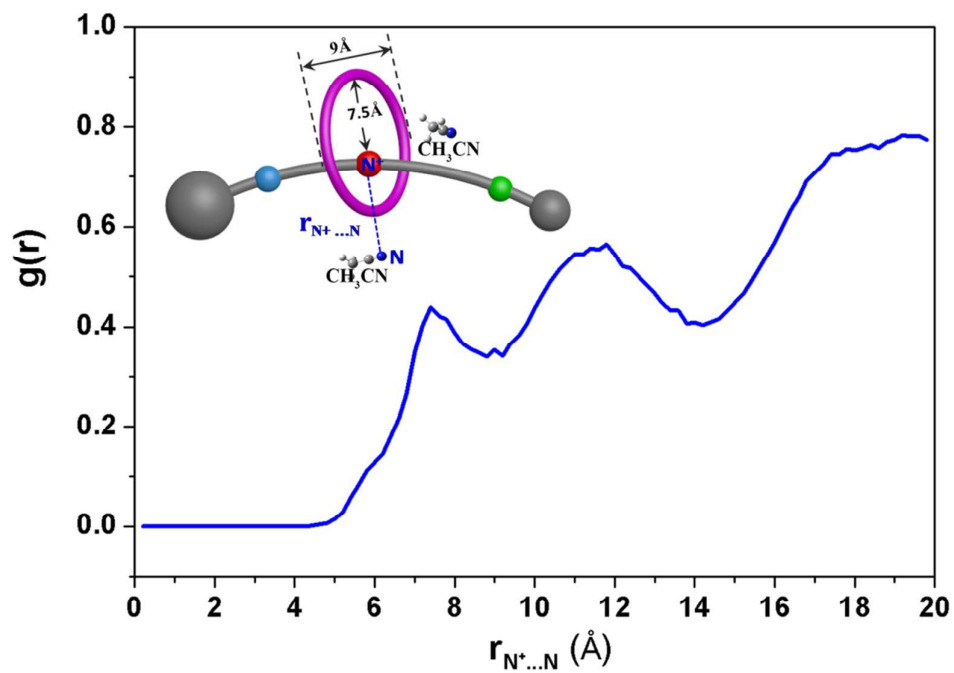


Figure S7. The radial distribution function of 1ns snapshot of MD simulation of Station I.